Leaf spring modeling

Niklas Philipson
Modelon AB
Ideon Science Park SE-22370 Lund, Sweden
niklas.philipson@modelon.se

Abstract

Although leaf springs are one of the oldest suspension components they are still frequently used, especially in commercial vehicles. Being able to capture the leaf spring characteristics is of significant importance for vehicle handling dynamics studies. The conventional way to model leaf springs is to divide the spring into several rigid links connected to each other via rotational stiffnesses. This can easily be done with the Modelica Standard Library, but it results in hard-to-use models with long simulation times. The models in this paper are designed as generalized force elements where the position, velocity and orientation of the axle mounting gives the reaction forces in the chassis attachment positions.

Keywords: Leaf spring; Vehicle dynamics; Commercial vehicle suspensions

1 Introduction

The commercial VehicleDynamics Library [1] is currently undergoing expansions to suite heavy vehicles (figure 1), requiring models of new components such as leaf springs. This paper covers one technique to generate a leaf spring that has good simulation performance and still captures the following characteristics.

- The axle attachment position will deflect in an arc shape in the longitudinal-vertical plane under vertical loading conditions [3].
- Leaf spring suspension designs have two anti roll bar effects. The springs are stiff in roll (twist) which counteracts the vehicles roll motion if the spring is mounted to a rigid axle as in figures 8 and 10. If the axle is mounted asymmetrically, that is not centered on the middle of the spring, the axle will twist as the vehicle rolls. This will resist vehicle roll as well [4].
- The effective length of the leaf spring varies with deflection causing a varying spring rate. The models in this paper require large deflections for the effect to be seen, but this effect can be higher for other shapes and mounting types of the spring [3].

The basic idea for the model is to use five massless links connected with rotational elasticities with the axle mounted at the center of the middle link. A massless approximation is reasonable since the masses involved in rigid axles, wheels and the body of the vehicle are considerably higher than the mass of the leaf spring. The implemented leaf spring can easily be extended with masses connected to the frames at the leaf springs three mounting positions. The shape of the

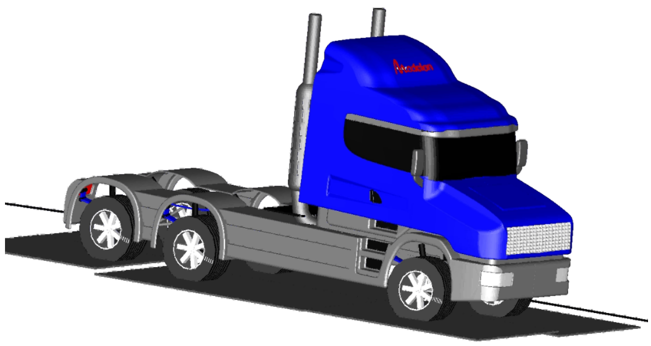

Figure 1: Tractor with leaf spring suspension in a shaker rig

leaf spring will be determined by the rotations between each link, except for the roll angles. These angles are left out of the equations of motion since they have very little impact on the leaf spring's shape. The roll resistance is handled as a rotational stiffness added to the torque equilibrium equations instead.

2 Reference MultiBody model

The model used as a basis for comparison is designed with components from the Multi-body package. The model consists of six rigid links connected by rotational stiffnesses that allow the center position to deflect in a plane. This design forms a planar loop and is only useful for vertical plane comparison.

Figure 2 illustrates a primitive suspension model assembled from two multi-body leaf springs. A translational joint is used to handle the distance variations in length between the mounting positions against the leaf springs. A spring is applied to the translational joint to control the lateral motion of the axle. The simulation time increases significantly with a stiffer translational spring. A more realistic model can be assembled by adding revolute joint for the lateral and roll motion as well, but the simulation time for just one planar leaf spring is already long.

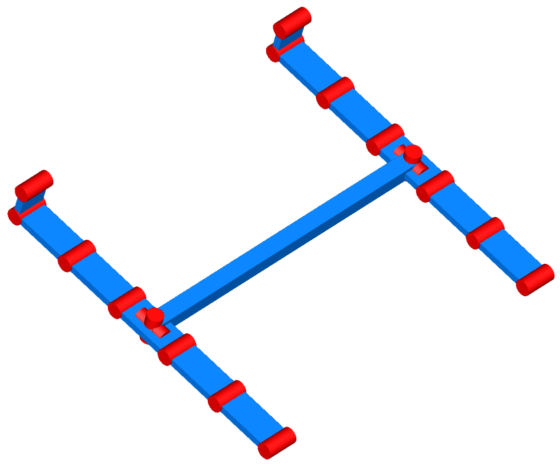

Figure 2: Multi body rigid axle suspension

3 Equations of motion

Lagrange's method, equation (1), is used to derive the equations of motion resolved in the generalized coordinates $(p1_y \dots p4_y, p1_z \dots p4_z)$ as illustrated in figure 3. Together with the stiffnesses indicated in figure 4, these form the expressions for the potential energy U in equation (2).

$$\frac{dL}{dt}\frac{\partial L}{\partial \dot{q}} - \frac{\partial L}{\partial q} + \frac{\partial R}{\partial \dot{q}} = F_{q_i} \qquad (1)$$

$$L = T - U \qquad (2)$$

In the sequel, it is assumed that the spring is massless giving $T = 0$. Viscous damping is applied over the generalized coordinates, giving

$$R = \sum_{i=1}^{i} \frac{1}{2} \cdot d_i \cdot \dot{q}_i^2 \qquad (3)$$

where q_i and d_i denotes each generalized coordinate and the corresponding damping coefficient.

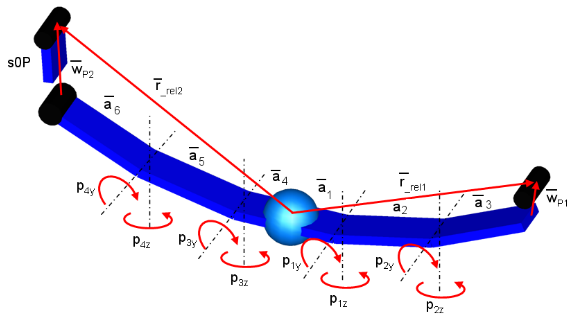

Figure 3: Definition of generalized coordinates and geometry properties.

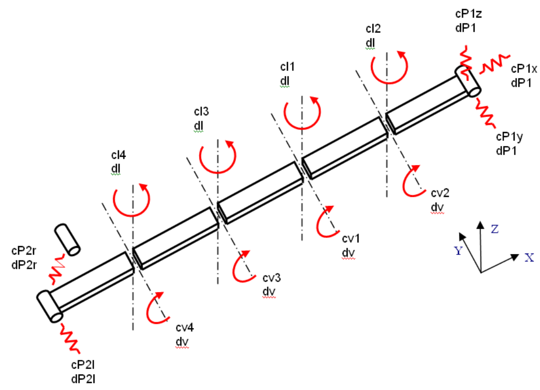

Figure 4: Parameters for stiffness and damping.

The potential energy stored in the spring is given by

$$\begin{aligned} U = {} & \frac{1}{2}\, c_{P1_x}\, w_{P1_x}^2 + \frac{1}{2}\, c_{P1_y}\, w_{P1_y}^2 + \frac{1}{2}\, c_{P1_z}\, w_{P1_3}^2 \\ & + \frac{1}{2}\, cv_1\, p2_y^2 + \frac{1}{2}\, cv_2\, p2_y^2 + \frac{1}{2}\, cv_3\, p3_y^2 \\ & + \frac{1}{2}\, cv_4\, p4_y^2 + \frac{1}{2}\, cl_1\, p1_z^2 + \frac{1}{2}\, cl_2\, p2_z^2 \\ & + \frac{1}{2}\, cl_3\, p3_z^2 + \frac{1}{2}\, cl_4\, p1_z^2 + \frac{1}{2}\, c_{P2_l}\, w_{P2_l}^2 \\ & + \frac{1}{2}\, c_{P2_r}\, w_{P2_r}^2 \end{aligned} \qquad (4)$$

where $w_{P1_{x,y,z}}$ and $c_{P1_{x,y,z}}$ are the displacements and stiffnesses of the front eye bushing. $w_{P2_{r,l}}$ denote the lateral and radial displacement of the shackle with $c_{P2_{r,l}}$ as the corresponding stiffnesses.

A non linear bushing description including a linear and a cubic stiffness gives the forces

$$F = \int_0^w \underbrace{k_1 \cdot w^2 + k_2}_{c} \, dw \tag{5}$$

and the potential energy

$$E = \int_0^w F \, dw \tag{6}$$

which can be used in equation (2) instead of the linear model. The forces will in this case depend on

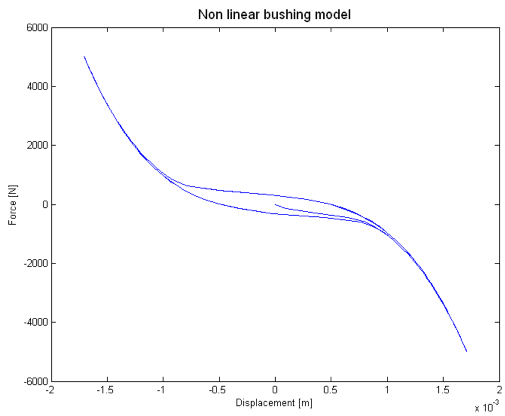

Figure 5: Force deflection diagram for front bushing

$c_{(p1y,p2y,p1z,p2z)}$ and $w_{(p1y,p2y,p1z,p2z)}$ for the front bushing. This results in a force deflection diagram for the front bushing seen in figure 5.

The displacements for the front eye bushing and the shackle are given by

$$\begin{aligned} \bar{w}_{P1} = \bar{r}_{rel1} - (&\bar{a}_1 + T_{y1} \cdot T_{z1} \cdot \bar{a}_2 \\ &+ R_{y1} \cdot R_{z1} \cdot T_{y2} \cdot T_{z2} \cdot \bar{a}_3) \end{aligned} \tag{7}$$

and

$$\begin{aligned} \bar{w}_{P2} = \bar{r}_{rel2} - (&\bar{a}_4 + T_{y3} \cdot T_{z3} \cdot \bar{a}_5 \\ &+ T_{y3} \cdot T_{z3} \cdot T_{y4} \cdot T_{z4} \cdot \bar{a}_6) \end{aligned} \tag{8}$$

respectively. Since the leaf spring is assumed to be rigidly mounted to the axle, it is convenient to resolve the equations for motion and force balance in the axle frame. The vectors $\bar{r}_{rel1}$ and $\bar{r}_{rel2}$ are expressed in the axle frame's coordinate system. The transformation matrices used to describe the end positions depending on the generalized coordinates used in equation (7) and (8) are given by

$$T_y = \begin{pmatrix} \cos(pX_y) & 0 & \sin(pX_y) \\ 0 & 1 & 0 \\ -\sin(pX_y) & 0 & \cos(pX_y) \end{pmatrix} \tag{9}$$

and

$$T_z = \begin{pmatrix} \cos(pX_y) & -\sin(pX_y) & 0 \\ \sin(pX_y) & \cos(pX_y) & 0 \\ 0 & 0 & 1 \end{pmatrix} \tag{10}$$

where X represents the respective generalized coordinate. L from equation (2) is now completely described with the eight generalized coordinates and the stiffness parameters. When solving equation (1) with respect to the generalized coordinates, two sets of non-linear equations appear. Since these sets do not depend on each other but only are a function of the axle's position, they can be used separately if there is a need to model half a leaf spring in conjunction with, for instance, an air spring.

The complexity of the equation system increases rapidly with added degrees of freedom. If, for instance, roll stiffness is added to the leaf spring in the same way as the other elasticities, it will expand the equation systems from two systems with four unknowns to two systems with six unknowns. Each expression in the equation systems will also expand since equations 7 and 8 must be modified with additional transformation matrices for the roll angles.

Instead of adding the roll degree of freedom, the roll torque is added externally as described in the next section by terms in equation 17 and 18. This approach is considered valid since the roll angles are small under normal operation conditions and the spring is relatively stiff in roll compared to the bushings.

Five links seem to be a reasonable compromise that achieve a fast simulated model but still captures the essential spring characteristics, this discretization is also used in [2]. Possibly, a larger number of links could be used if the equations of motion were to be linearized. This might cause problems with the initial curvature which requires large angles between the links.

4 Force generation

The displacements and the displacement's derivative together with the stiffness and damping coefficients give the forces in the mounting positions to the chassis. The forces in the chassis mounts are given by equation (11) and (14),

$$\bar{f}_{P1} = \mathbf{C}_{P1} \cdot \bar{w}_{P1} + \bar{\dot{w}}_{P1} \cdot d_{P1} - \bar{f}_{0P1} \tag{11}$$

$$f_{P2_r} = c_{P2_r} \cdot (w_{P2_r} - sP0) + \dot{w}_{P2_r} \cdot d_{P2_r} - f_{0P2_z} \tag{12}$$

$$f_{P2_l} = c_{P2_l} \cdot w_{P2_l} + \dot{w}_{P2_l} \cdot d_{P2_l} \tag{13}$$

$$\bar{f}_{P2} = f_{P2_r} \cdot \hat{n}_{P2_r} + f_{P2_l} \cdot \hat{n}_{P2_l} \tag{14}$$

where **C** is a diagonal $(3x3)$ matrix with the translatory stiffnesses for the front eye bushing. The damping of the front bushing is currently set as one value for all directions. $\hat{n}_{P2_{l,r}}$ denote unit vectors in the radial and lateral directions of the shackle. The length of the shackle used for describing the shackles radial displacement in equation (12) is named $s0P$.

The force and torque equilibria are given by

$$\bar{0} = \bar{f}_{P4} + \bar{f}_{P1} + \bar{f}_{P2} \tag{15}$$

and

$$\bar{0} = \bar{t}_{P4} + \bar{t}_{P1} + \bar{t}_{P3} + \bar{r}_{rel1} \times \bar{f}_{P1} + \bar{r}_{rel2} \times \bar{f}_{P3} \tag{16}$$

respectively. The roll stiffness is modeled as a rotational spring and added to the torque equilibrium. The roll angle is the only variable that has an impact on the torque acting on the front bushings. This gives

$$p_r \cdot c_r \cdot \hat{n}_x = \bar{t}_{P1}. \tag{17}$$

as the resulting torque. The force is calculated in the lower shackle mount and must be transformed as

$$\bar{t}_{P2} = \bar{f}_{P3} \times \hat{n}_{P2} \cdot s_{0P} + p_r \cdot c_r \hat{n}_x \tag{18}$$

.p_r is the spring's roll angle with the corresponding rotational stiffness c_r. The unit vector in the x direction of the axle frame's coordinate system is denoted $\hat{n}_x$.

5 Implementation

The primitive model of the leaf spring requires geometry positions in a two dimensional plane. For the model to be useful, a wrapper is needed to translate the initial three dimensional positions to parameters for the leaf spring. This is done according to equation 22 though 29. The location of the primitive model's

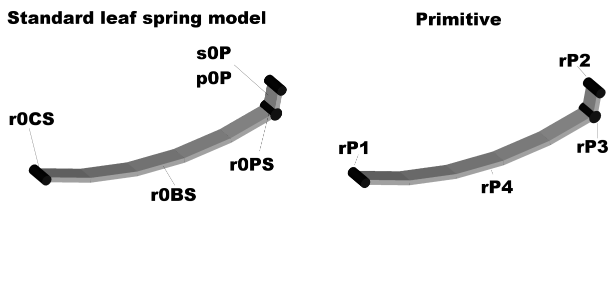

Figure 6: Leaf spring primitive and wrapped model

hard points are illustrated in figure 6.

The transformation matrix T in which the planar positions are resolved is given by the base vectors (nx, ny).

$$\bar{nx} = \bar{r}_{0CS} - \bar{r}_{0PS} \tag{19}$$

$$\bar{ny} = (\bar{r}_{0PS} - \bar{r}_{0BS}) \times (\bar{r}_{0CS} - \bar{r}_{0BS}) \tag{20}$$

Equation (20) is unsolvable when the vectors are parallel. This is taken care of by an assertion which encourages the user to enter ny manually.

$$\bar{r1} =^T (\bar{r}_{0PS} - \bar{r}_{0CS}) \tag{21}$$

$$\bar{r2} =^T (\bar{r}_{0BS} - \bar{r}_{0CS}) \tag{22}$$

The vectors $(r1, r2)$ resolved in T have y-values equal to zero, and can thus be used to extract the positions for the four hard points used in the primitive model according to equations (23) though (26).

$$\bar{r_{P1}} = \bar{0} \tag{23}$$

$$\bar{r}_{P2} = \bar{r}_{P3} + s0P \cdot (sin(p_{0P}), cos(-p_{0P})) \tag{24}$$

$$\bar{r}_{P3} = (r1_x, r1_z) \tag{25}$$

$$\bar{r}_{P4} = (r2_z, r2_z) \tag{26}$$

The leaf spring's curvature is defined as $1/R$ where R is the radius of the leaf springs shape. The implemented models have a curvature that depends on the hard points for the three mounting positions. There is one curvature for the rear part generated from the axle and the lower shackle mounts position and one for the front part generated in the same way as for the rear.

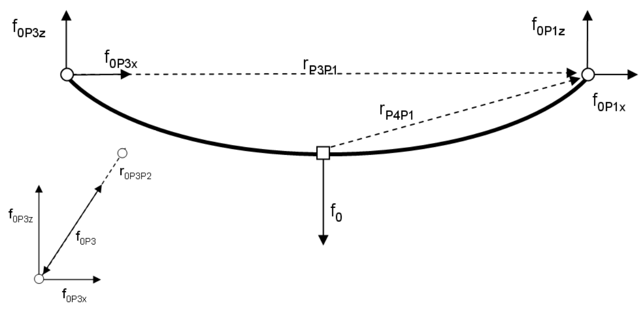

Figure 7: Pretension forces

To enable an easy way to determine the shape of the leaf spring and the ride height of the vehicle at the design configuration it is necessary to specify a pretension value corresponding to the load when the vehicle is at rest. The forces from pretension are given by

$$f_{0P1_x} + f_{0P3_x} = 0 \tag{27}$$

$$f_{0P1_z} - f_0 + f_{0P3_z} = 0 \tag{28}$$

$$f_{0P3_z} \cdot r_{P3P1_x} - f_{0P3_x} \cdot r_{P3P1_z} - f_0 \cdot r_{P4P1_x} = 0 \qquad (29)$$

$$f_{0P3_z} = f_{0P3} \cdot -\frac{r_{0P3P2_z}}{|r_{0P3P2}|} \qquad (30)$$

$$f_{0P3_x} = f_{0P3} \cdot -\frac{r_{0P3P2_x}}{|r_{0P3P2}|} \qquad (31)$$

and indicated in figure 7. These forces are calculated initially and added as static values in equation (11) and (12).

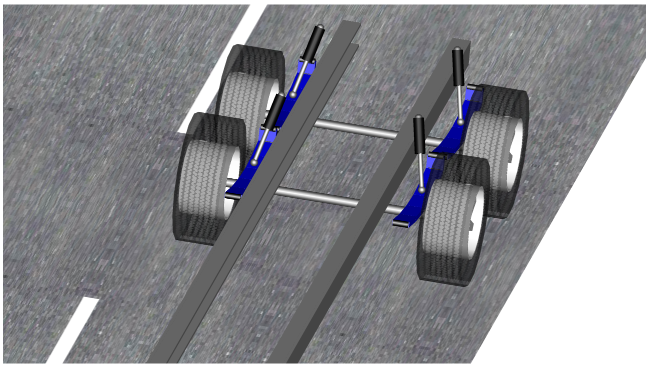

Figure 8: Semi trailer boogie suspension

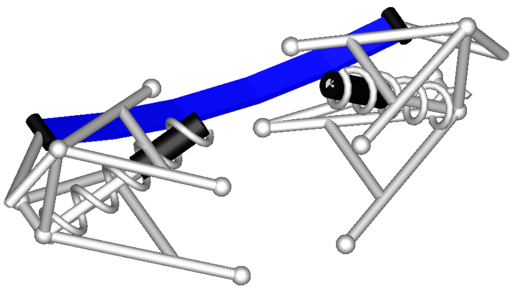

Figure 9: Leaf spring and double wishbone suspension

The implemented leaf spring models can be used in numerous designs, here presented in a semi trailer boogie suspension, figure 8, and in a double wishbone design, figure9. One of the axles in the semi trailer suspension is assembled as shown in figure 10. Figure 9 illustrates another leaf spring model without a shackle mounted between two wishbones and with the center attachment mounted to the chassis. This model is based on the same technique as the standard leaf spring model.

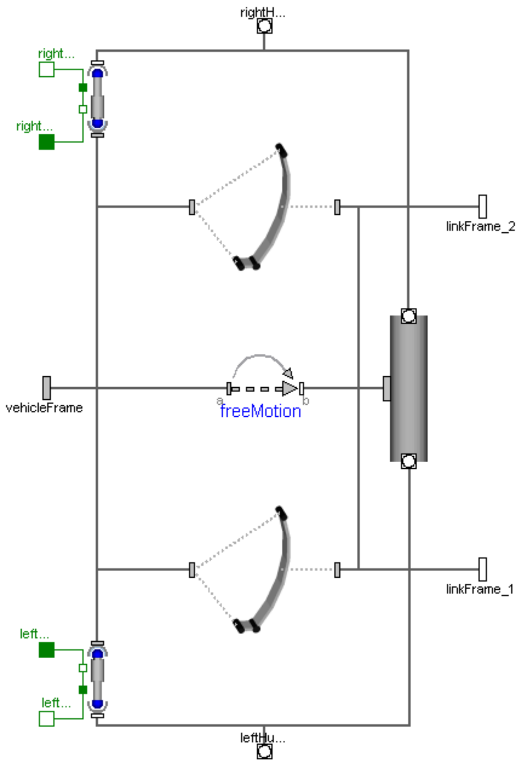

Figure 10: Diagram view of leaf spring axle carriage

6 Parametrization

The parameters needed for the leaf spring consists of positions, stiffnesses, dampings, and animation properties.

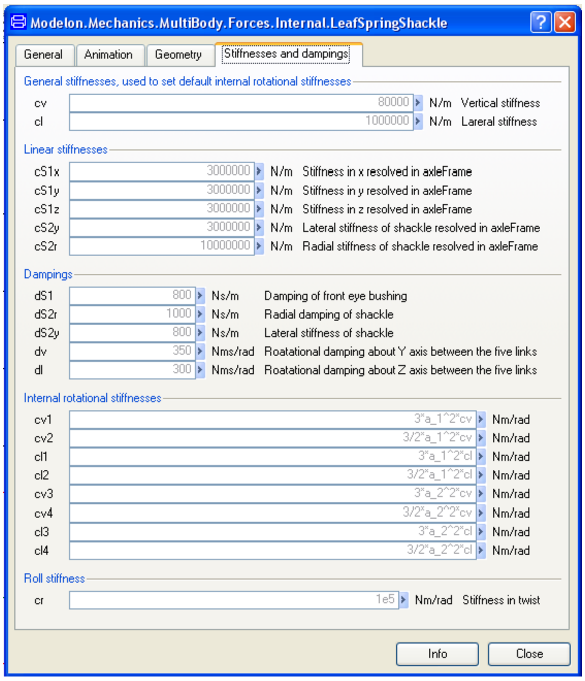

Figure 11: Elasticity parameters

Figure 11 displays the elasticity parameters for the primitive model. The default value for the internal rotational stiffnesses are calculated from the vertical and lateral stiffness under the assumption that the leaf spring will deflect in the shape of an arc. The internal rotational stiffnesses can be set manually to enable the user to customize the deflection profile.

The parametrization can easily be changed to suite different specific types of leaf springs in terms of shape and asymmetric stiffness.

7 Validation and results

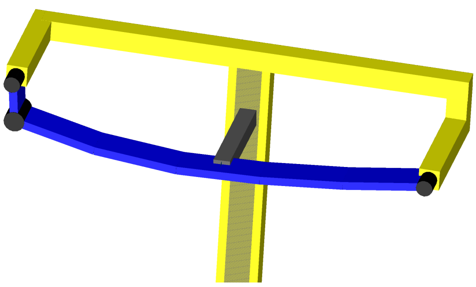

Figure 12: Leaf spring test rig

The validation of the standard leaf spring has been carried out by comparing the model to a reference multi-body model described in section 2. A test rig, figure 12, has been used to generate the dynamic and kinematic comparison. As seen in figure 13 the vertical plane kinematics of the leaf spring modeled with rigid elements are virtually the same as for the model described by Lagrange's equation. Both models are damped via viscous damping over each generalized coordinate and corresponding revolute joint for the multi-body model. The vertical plane dynamics for the different models are very similar to each other as long as the excitation does not consist of high frequency components as in figure 14.

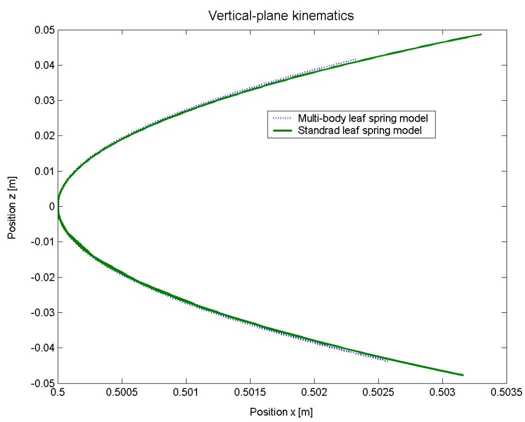

Figure 13: Vertical plane kinematics comparison

The fact that the standard model has both stiffness and damping in the mount positions makes it a bit complicated to compare these results, but without fine tuning of the stiffness and damping they perform as shown in figure 13.The differences can easily be related to the bushings in the mount positions and the massless approximation used in the standard leaf spring.

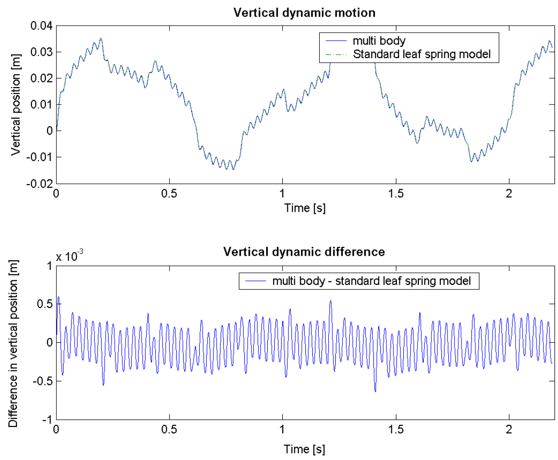

Figure 14: Vertical plane dynamics

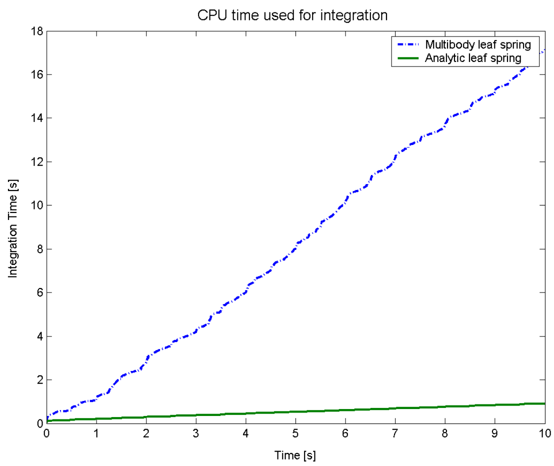

Figure 15: Cpu time used for simulation of the different suspension models

A suspension assembled as in figure 10 simulates approximately 18 times faster then the reference suspension, as shown in figure 15.

A comparison of the kinematic and dynamic behavior of two multi body leaf springs with five versus

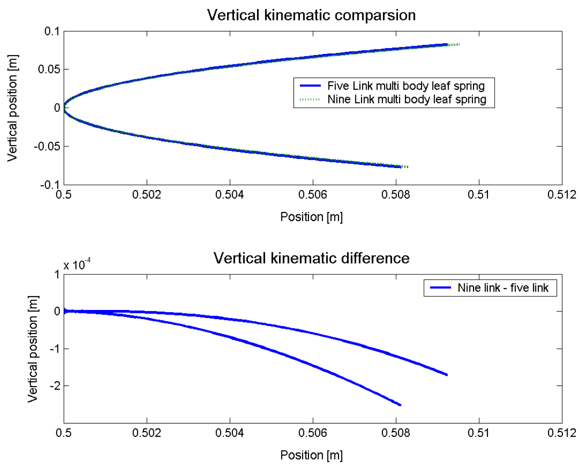

Figure 16: Kinematic comparsion between nine and five link leaf spring

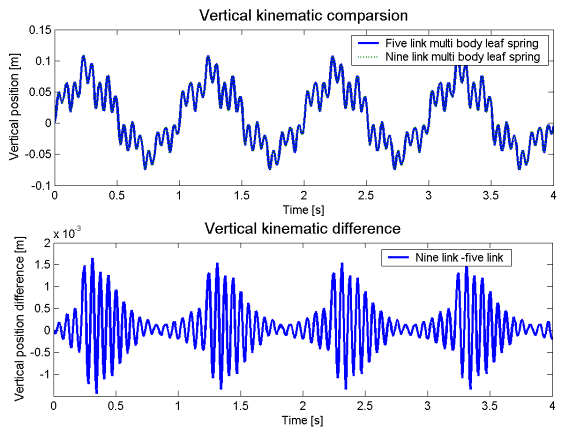

Figure 17: Dynamic comparison between nine and five link leaf spring

nine links is illustrated in figure 16 and 17. The differences between the models are small which implies that the five link leaf spring meets the requirements for vehicle handling simulations.

The shackle has big influence on the leaf spring's kinematics. The shape of the leaf spring in the comparison results in larger deflection in bounce than in rebound, figure 16. This because the shackle's lower mount towards the spring always moves upwards with deflection. Other geometries would give different results.

8 Summary

The leaf spring model is essential for heavy vehicle handling dynamics simulations. The proposed model is superior to the multi-body reference model with respect to simulation time and it is much easier to parameterize the geometry positions and to implement it in suspension designs. The model is equipped to deal with the specific characteristics of a leaf spring. It is possible to add forces through the same equations as the pretension but varying over time. This enables a user to add additional force elements as damping via hysteresis or air springs. The standard leaf spring model fulfills all the requirements specified in section 1.

References

[1] *J. Andreasson, M. Gävert*. The VehicleDynamics Library — Overview and Applications Modelon., Homepage: http://www.modelon.se/. In *Proceedings of Modelica'2006*, Vienna, Sep. 2006.

[2] *Georg Rill, Norbert Kessing, Olav Lange* and *Jan Meier:* Leaf Spring Modelling for Real Time Applications In the *18th IAVSD-Symposium in Atsugi, Japan 2003*, 2003.

[3] *SAE:* Spring Design Manual ISBN: 1-56091-680-X, 1996.

[4] *A grimm, C. Winkler* and ,*R. Sweet* Mechanics of Heavy Duty Truck Systems. University of Michigan transportation research institute, UK , 2004.